Plasmonic Crystal-Based Gas Sensor Toward an Optical Nose Design

Shawana Tabassum, Ratnesh Kumar, *Fellow, IEEE*, and Liang Dong

***Abstract*— This paper presents a high-sensitivity gas sensor based on plasmonic crystal incorporating a thin layer of graphene oxide (GO). The plasmonic crystal consists of a periodic array of polymeric nanoposts with gold (Au) disks at the top and nanoholes in an Au thin film at the bottom. The thin GO layer coated atop the plasmonic crystal is the gas absorbent material for the sensor. Gas adsorption of GO modifies the refractive index of the plasmonic structure and returns a shift in the resonance wavelength of the surface plasmon polariton excited at the GO coated Au surface. The differences in target gas species and their adsorption in GO lead to a difference in the resonance shift. To identify the gas species in a complex gas mixture, a sensor array is designed with different sensing elements coated with different thicknesses of GO. The optical responses of the different sensing elements to a gas mixture are analyzed using principal component analysis (PCA)-based pattern recognition algorithm. The PCA separates the sensor responses to different species of gases, providing specificity of the device. The proposed sensor demonstrates a refractive index sensitivity of 449.63 nm/RIU. In addition, volatile organic compounds, such as ethylene, methanol that serve as plant health indicators and ammonia that plays a key role in the ecosystem, are detected by the sensor. A change in a gas concentration results in a differing amount of adsorbate and correlated shift in the resonance wavelength of the device. The GO coated sensor exhibits sensitivities of 0.6 pm/ppm to gaseous ethylene, 3.2 pm/ppm to methanol, and 12.84 pm/ppm to ammonia. The integration of plasmonic sensing element arrays with varying GO thicknesses to modulate the gas adsorption, offers a promising approach to detect different gas species in a single test.**

***Index Terms*— Gas sensing, surface plasmon resonance, graphene oxide, principal component analysis.**

I. Introduction

WE PRESENT an "optical nose" for sensing gases, especially the ones useful as plant health indicators such as ethylene, methanol, and ammonia. Plant growth and development are profoundly influenced by several chemical substances including ethylene and methanol. Ethylene regulates cell size and cell division, initiates the fruit ripening process and accelerates senescence of leaves [1], [2]. Methanol, on the other hand, is responsible for early stages of plant leaf development [3]. Plants emit ethylene and/or methanol during different stages of development as well as when plants respond to environmental stimuli from biotic and/or abiotic stresses [4]. Measuring the presence and concentration of these gases released by plants is of utmost importance to carefully monitor the condition of fruits and vegetables, and significantly prevent their wastage due to over-ripening. Furthermore, gaseous ammonia (NH_3) emission from plant's foliage and shoots bears a measurable impact on the biotic as well as abiotic components of our ecosystem. Exchange of ammonia between the atmosphere and plants plays a significant role in flora decline due to for example excessive nitrogen deposition. Thus, detecting concentrations of NH_3 can help monitor environmental health. The importance of ethylene and methanol in plant development and of ammonia in healthy ecosystem makes it imperative to develop highly sensitive and selective gas sensors for their monitoring.

An ethylene gas sensor utilizing carbon nanotube [1] and an indium tin oxide (ITO) thin film based methanol gas sensor [5] have been reported. These sensors work on the basis of the conductance/resistance variation upon the adsorption of gas species on their surface. A number of surface plasmon resonance (SPR) based optical sensors have been reported for the detection of ammonia [6]–[8]. Numerous optical gas sensors have also been reported by integrating optical resonators and gas absorption materials, or using optical resonators alone. Polymers such as silicone rubber, polyvinylchloride (PVC), and polytetrafluoroethylene with immobilized gas sensitive chemical reagents were used in optical sensors to detect various gases [9]. Localized surface plasmon resonance (LSPR) at the surface of gold (Au) and silver nanoparticles, and gold nanoshells allowed the detection of gas-molecular-binding-induced changes of refractive index [10]. Au nanoparticles were also coupled with reduced graphene oxide (rGO) to generate LSPR for gas sensing [11]. Fiber-optic sensors that eliminate bulky optics and offer easy insertion of device into the sensing area have also been reported: An SPR based chlorine gas sensor was realized by applying indium oxide doped tin oxide to the surface of silver-coated optical fiber core [12]. In addition, an SPR based fiber-optic ammonia gas sensor was designed using a tin-oxide (SnO_2) layer over the silver-coated unclad core of the fiber [6]. Other works studied nanocomposite films of poly (methyl methacrylate) (PMMA), rGO and PMMA/rGO [7], polyaniline coated ITO thin film [8], graphene-carbon nanotubes-poly(methyl methacrylate) hybrid nanocomposite [13], and ITO thin film and nanoparticles [14] to develop SPR based fiber-optic gas sensors. Also, various photonic crystal (PC)-based resonators were developed for

Manuscript received August 1, 2017; accepted August 10, 2017. Date of publication August 15, 2017; date of current version September 8, 2017. This work was supported in part by the U.S. National Science Foundation under Grant CCF-1331390 and Grant IIP-1602089, and in part by ISU's Regents Innovation Fund. The associate editor coordinating the review of this paper and approving it for publication was Dr. Camilla Baratto. *(Corresponding author: Shawana Tabassum.)*

The authors are with the Department of Electrical and Computer Engineering, Iowa State University, Ames, IA 50011 USA (e-mail: tabassum@iastate.edu; rkumar@iastate.edu; ldong@iastate.edu).

Digital Object Identifier 10.1109/JSEN.2017.2740176

the detection of volatile organic compounds (VOCs) [15], under the principle of index modulation upon vapor adsorption and condensation inside the PCs. The extremely high quality factor of whispering gallery mode (WGM) was also utilized to generate resonance shift caused by specific binding of gas molecules through enhanced photon-gas molecule interactions [16]. Furthermore, chalcogenide glass waveguides have been used for gas detection due to their very high refractive index (2.0-4.0) and transparency in the mid-infrared spectral regime [17].

Notably, resonant characteristics of surface plasmon polariton (SPP)-based nanostructures are sensitive to subtle changes in surrounding refractive index, and thus, are finding sensor applications for the detection of chemical and biological species [18]. These nanostructures are mostly limited to liquid-phase detection of biomolecules such as protein [19], DNA [20], cancer biomarkers [21] and glucose [22]. However, due to the lack of suitable absorption materials for detecting gas molecules, it remains challenging to generate a large output signal in response to minute concentration of gas. Recently, GO has led to the development of many ultrasensitive sensors owing to high surface-area-to-volume ratio [23] and sufficient functional groups (e.g., carboxyl, hydroxyl, carbonyl and epoxide) at the surface of GO nanosheets providing effective trap centers for various gas species [24]. Several electronic gas sensors have used GO and GO-based nanocomposites for gas detection [25], [26], where their electrical conductivities change upon exposure to gases. To date, there are limited reports on integrating GO as a sensing material with SPP-based nanostructures for the detection of gas molecules [27]. In addition, the utilization of principal component analysis (PCA) to separate the gas species and improve specificity is an integral feature in our sensing approach.

In this paper, we report an optical gas sensor utilizing enhanced gas adsorption ability of GO and the strong light-matter interaction at the surface of lithographic plasmonic nanoposts. The plasmonic nanostructures are composed of an array of nanoposts with Au disks at the top and perforated nanoholes in an Au thin film at the bottom. The nanostructures are coated with a thin layer of GO nanosheets to form a sensitive adsorption surface for gas molecules, and support the excitation of SPPs at the dielectric/Au interface with a high refractive index sensitivity. More importantly, to distinguish different types of gaseous species, an array of nanostructured sensors is designed, where the surface of each individual sensor is coated with a different thickness of GO. Depending on the GO coating thickness, the amount of gas molecules absorbed by GO varies, leading to a different modulation for the effective refractive index of GO at different sensing elements when responding to a specific gas species. This allows for the selective identification of gas species by integrating a pattern recognition algorithm such as PCA algorithm [28].

II. Sensor Design and Working Principle

The GO coated plasmonic crystal sensor is shown in Fig. 1a. The nanoposts made of a ZPUA (ZIPCONE™UA) polymer have a square lattice with the period of 500 nm, the diameter of 250 nm, and the height of 210 nm. The surface of the sensor is coated by 5 nm thick titanium and 50 nm thick Au. The device was formed using soft lithography based replica nanomolding process. The details of fabrication processes appear in Supplementary Materials at the end in an appendix. To enhance the specificity of this sensor to different gas species, an array of three sensors was formed on the same substrate, by coating with three different thicknesses of GO: 16.3 nm, 32.6 nm, and 48.9 nm. This sensor array was used to examine the response of the sensors to gaseous ethylene, methanol and ammonia.

A. Working Principle

When gas molecules are adsorbed at the surface of GO nanosheets, the hydroxyl and carboxyl groups at the basal planes and edges of GO form oxo- or hydroxo-bridges with the gas molecules. This results in free electron transfers between the GO nanosheets and gas molecules. The change in conductivity of GO in response to its interaction with gas molecules can be written as [29],

$$\Delta\sigma_{GO}(t) = \Delta\sigma_{max,GO}\frac{cK}{1+cK}[1-\exp(-\frac{1+cK}{K}kt)] \quad (1)$$

where $\Delta\sigma_{GO}$ is the change in conductivity of GO, $\Delta\sigma_{max,GO}$ is the maximum change in conductivity with sufficient gas exposure, K is binding equilibrium constant, k is surface reaction rate constant, c is the concentration of gas and t is the time for gas exposure. The refractive index of GO, η_{GO} is calculated from the following equation [30], [31],

$$\eta_{GO} = (\frac{1}{2\omega\varepsilon_0 t_{GO}})^{1/2}(-\sigma_{GO,i} + \sqrt{4\sigma_{GO,r}^2 + \sigma_{GO,i}^2})^{1/2} \quad (2)$$

where, ω is the angular frequency, $\varepsilon_0 = 8.85 \times 10^{-12}$F/m and t_{GO} is thickness of the GO nanosheet. It can be observed from (1) and (2) that η_{GO} is related to gas concentration c, and higher the value of c, higher the value of η_{GO}. These equations explain how η_{GO} varies when the GO nanosheet is exposed to gases of varying concentrations. The variation in η_{GO} causes shifts in the resonance wavelengths of surface plasmons, as explained below, and that shift is what we measure experimentally.

Under normal incidence, the free space light to excite a SPP at the dielectric/metal interface for a square lattice is given by the following equation [32]:

$$\lambda_{SPP} = \frac{\Lambda}{\sqrt{i^2+j^2}}\sqrt{\frac{\varepsilon_d\varepsilon_m}{\varepsilon_d+\varepsilon_m}}, \quad (3)$$

where ε_d and ε_m are the dielectric constants of the dielectric and the metal (Au in our work), respectively, Λ is the lattice period, and (i, j) is the order of SPP. For the proposed structure, $\Lambda = 500$ nm and when the Au nanostructures are coated with a thin layer of GO nanosheets, $\varepsilon_d = (\eta_{GO})^2$. Hence, in presence of adsorbed gases with concentration c, η_{GO} varies according to the Equations (1) and (2), causing ε_d to vary, which in turn causes λ_{SPP} to shift. On the other hand, the relative permittivity of Au, $\varepsilon_m \equiv \varepsilon_m(\lambda)$ depends on wavelength and is taken from the experimental data [33].

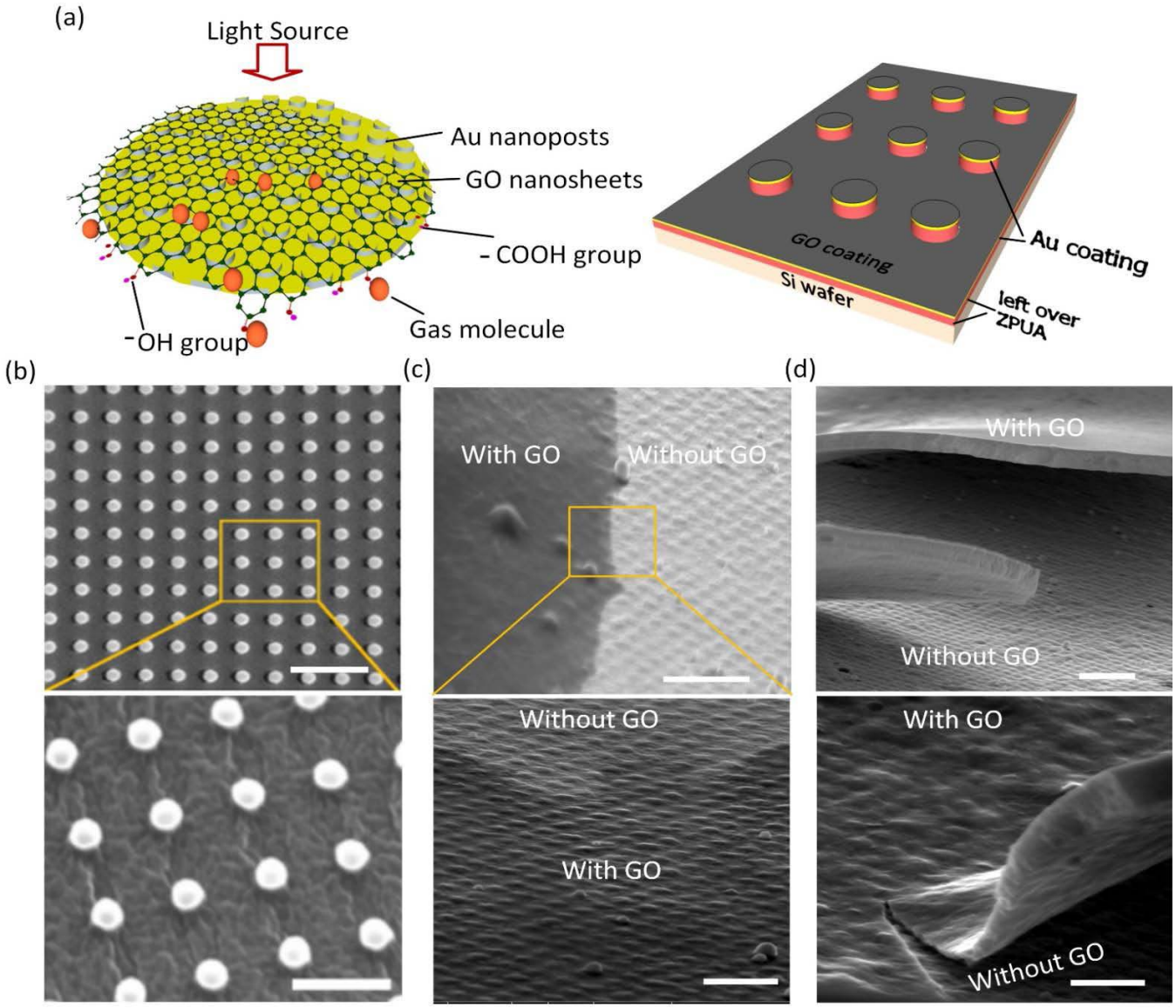

Fig. 1. (a) Schematic illustration of the GO coated plasmonic crystal sensor. (b) Top-view scanning electron microscopy (SEM) images of an array of polymer nanoposts (lattice constant = 500 nm, post diameter = 250 nm, post height = 210 nm) without Au coating. Scale bars represent 1 μm (top panel) and 500 nm (bottom panel). (c) 70° tilt-view of the nanopost array deposited with Au/GO coating. Scale bars represent 2 μm (top panel) and 1 μm (bottom panel). (d) 70° tilt-view of the GO nanosheet separated from the nanopost surface at the edge. Scale bars represent 2 μm (top panel) and 1 μm (bottom panel).

Equation (3) can be used to determine the resonance wavelength λ_{SPP} under the influence of index modulation of the surrounding medium. The equation cannot be solved directly because relative permittivity of Au is a function of wavelength, and so the wavelength appears on both sides of the equation. In order to compute the SPP resonance wavelength, left and right hand sides of (3) are plotted as a function of wavelength. From the intersection of the two curves, the calculated SPP resonance λ_{SPP} for $(i, j) = (1, 0)$ at the air/Au interface is 546.7 nm.

III. Experimental Results and Analysis

A. Characterization of Au/GO Coated Nanopatterns

A schematic of the GO coated sensor is given in Fig. 1a. The scanning electron microscopy (SEM) analysis was performed to provide a comprehensive characterization of the GO coated plasmonic nanostructure (Fig. 1b-d). The top-view SEM image of the bare nanopatterns (without Au or GO coating) is shown in Fig. 1b. After coating the device with a 50 nm thick Au layer followed by a coating of 0.2 mg/ml GO dispersion solution (0.2 mg GO in 1 ml DI water, preparation of which is given in the Supplementary Materials in an appendix at the end), a 70° tilt-view SEM image of the device was taken (Fig. 1c). The boundary between GO coated and uncoated device is clearly visible in Fig. 1c. It is also confirmed from the SEM image that the GO nanosheet is conforming to the structure beneath it. In order to reveal the thickness of the GO nanosheets, a 70° tilt-view SEM image was captured at the edge of the device where GO nanosheets got detached from the device surface (Fig. 1d).

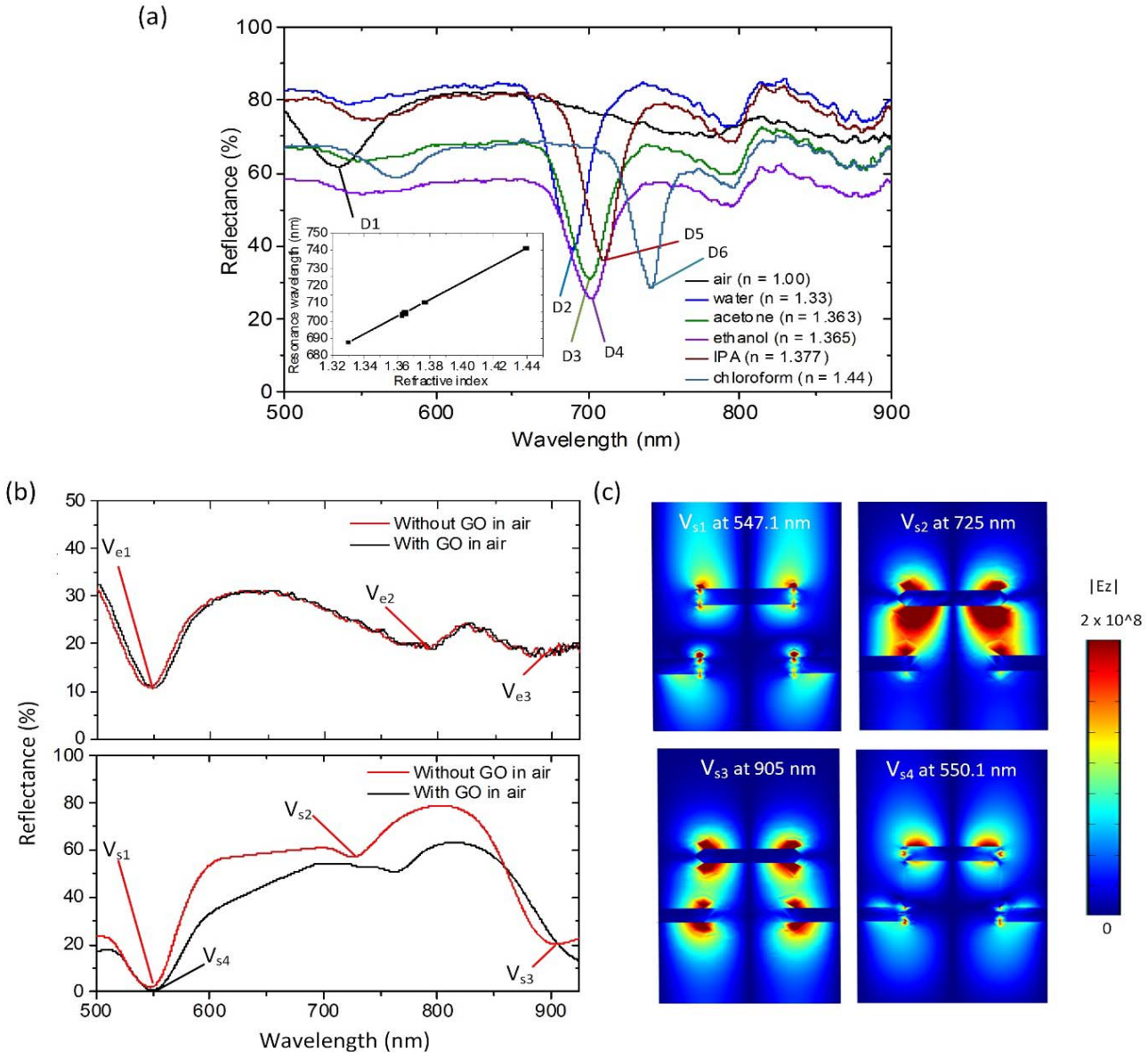

Fig. 2. (a) Reflectance spectra of bare structure (without GO) in response to air ($\lambda_{D1} = 547.1$ nm), water ($\lambda_{D2} = 688$ nm), acetone ($\lambda_{D3} = 700.8$ nm), ethanol ($\lambda_{D4} = 702.5$ nm), IPA ($\lambda_{D5} = 710.5$ nm) and chloroform ($\lambda_{D6} = 741.5$ nm). The inset shows refractive index sensitivity curve. (b) The measured (upper panel) and simulated (lower panel) reflection spectra of the plasmonic nanostructure without and with a 16.3 nm thick GO coating under normal incidence of light. V_{s1}, V_{s2}, V_{s3} and V_{s4} in the simulated spectra indicate the reflection features of interest. $\lambda_{Vs1} = 547.1$ nm, $\lambda_{Vs2} = 725$ nm, $\lambda_{Vs3} = 905$ nm and $\lambda_{Vs4} = 550.1$ nm. (c) Simulated cross-sectional electric field distribution at the SPP resonant wavelength of 547.1 nm, 725 nm and 905 nm without any GO coating, and at the SPP resonance wavelength of 550.1 nm with a 16.3 nm thick GO coating. The color bar shows field intensity.

B. Bulk Refractive Index Change Characterization

A bifurcated optical fiber (BIF 400-VIS-NIR, Ocean Optics) was used to illuminate the sensor from a white light source (150 watt quartz halogen lamp, Luxtec Fiber Optics) through a collimator (F220SMA-A, Thorlabs), and collect the reflected light from the sensor into a spectrometer (USB-4000, Ocean Optics). We measured the reflectance spectra with normal incident light. When the bare (without GO coating) plasmonic nanostructure was exposed to air, a reflectance dip appeared at 547.1 nm (Fig. 2a, D1), close to what was calculated using (3). Next, we performed the bulk refractive index sensitivity measurement of the Au-coated nanoposts without GO coating (Fig. 2a). Water ($\eta = 1.33$), acetone ($\eta = 1.363$), ethanol ($\eta = 1.365$), isopropyl alcohol (IPA) ($\eta = 1.377$), and chloroform ($\eta = 1.44$) were dropped on the top of the device and covered with a glass coverslip (Fig. 2a). As the surrounding medium changed from air to water, acetone, ethanol, IPA or chloroform, the resonance wavelength shifted from 547.1 nm (D1) to 688 nm (D2), 700.8 nm (D3), 702.5 nm (D4), 710.5 nm (D5) or 741.5 nm (D6) respectively (Fig. 2a). Thus, the sensor exhibited a refractive index sensitivity of 449.63 nm/RIU, shown in Fig. 2a inset.

C. Optical Simulations

Finite element analysis method was used to carry out full wave numerical simulations with the commercial COMSOL

software. Fig. 2b shows the experimental and simulated reflection spectra of the plasmonic nanostructure with and without the GO coating. A certain thickness (300 nm) of left-over ZPUA polymer beneath the nanoposts (Fig. 1a) was also incorporated in order to simulate the actual device. The resonance dip at $\lambda_{Vs1} = 547.1$ nm for the bare structure (without GO) corresponds to the excitation of (1,0) SPP at the air/Au interface. This is confirmed by the standing wave feature above the Au nanodisk and below the Au film as can be seen in the simulated electric field distribution (Fig. 2c). Moreover, it can be observed that the resonant field penetrates approximately 100 nm to the surrounding dielectric (e.g. air), which helps determine the thickness of GO coating to be used for gas adsorption and its interaction with the electric field distribution. Accordingly, the maximum thickness of the GO coating that we used was 48.9 nm, well below the observed field penetration depth into air of 100 nm. The strong interaction between the LSPRs at the Au nanodisk and Au film results in a Fabry-Pérot (FP) resonance at $\lambda_{Vs2} = 725$ nm (Fig. 2c). Such FP resonance has also been observed in [34]–[36]. The dip at $\lambda_{Vs3} = 905$ nm is due to a relatively weaker coupling between the LSPRs mentioned above (Fig. 2c). The three reflectance dips in the simulated spectrum (λ_{Vs1}, λ_{Vs2}, and λ_{Vs3}) correspond to the three dips (λ_{Ve1}, λ_{Ve2}, and λ_{Ve3}) in the experimental reflectance spectrum (Fig. 2b). However, the simulated reflectance dip λ_{Vs2} is slightly blue shifted with respect to the experimentally observed dip λ_{Ve2}. This may be attributed to the unknown thickness of left-over ZPUA in real device below the nanoposts. Because of the enhanced penetration of (1, 0) SPP resonant field into the surrounding dielectric compared to the LSPR fields, the shift in (1, 0) SPP resonance wavelength was measured in response to changes in surrounding refractive indices. After coating the device with a 16.3 nm thick GO layer, the (1, 0) SPP resonance wavelength of the device shifted from $\lambda_{Vs1} = 547.1$ nm (bare structure without any GO coating) to $\lambda_{Vs4} = 550.1$ nm (with GO coating) as shown in Fig. 2b. The figure also confirms that the measured and simulated results agree well with each other.

IV. Application to Gas Sensing

The GO coated plasmonic nanostructure was demonstrated to function as a gas sensor. To achieve selectivity, a combination of GO layer thickness variations together with a PCA based pattern recognition was employed. Varying the thickness provided varying reflection spectra responses that contained the signature of the gas species, whose extraction was achieved via the PCA. An array of three sensors was designed to have different response characteristics to gases owing to different thicknesses of the GO coating, namely, 16.3 nm, 32.6 nm, and 48.9 nm.

A. Chemical Interaction of Gases With GO

The hydroxyl, carboxyl and the epoxy groups present at the basal planes and edges of GO play a significant role in capturing gas molecules. The binding mechanism of NH_3, methanol and ethylene gases at GO nanosheets is illustrated in Fig. 3. NH_3 interacts with carboxyl groups as either Bronsted (Fig. 3a) or Lewis (Fig. 3b) acids [37]. NH_3 also reacts with the epoxy groups via nucleophilic substitution (Fig. 3c) and forms amide [37]. In a moist environment, water molecules form hydrogen bonds with the hydroxyl and epoxy groups present between GO layers leading to less amount of NH_3 adsorption. In dry condition (in the absence of H_2O molecules), NH_3 binding with the hydroxyl and epoxy groups is significantly enhanced. Methanol also works as a nucleophile that attacks the carboxyl groups at GO and forms ester (Fig. 3d) [38]. When the GO nanosheets are exposed to ethylene, it attacks the hydroxyl groups at GO via nucleophilic substitution (Fig. 3e) [39].

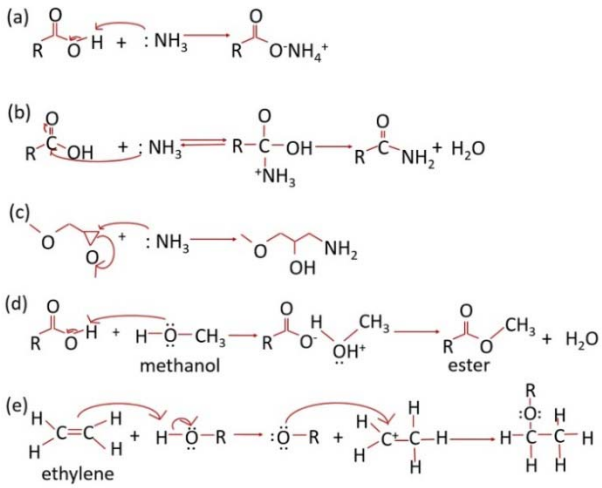

Fig. 3. Mechanism of interaction of NH_3 (a,b,c), methanol (d), and ethylene (e) gases with the functional groups present at GO nanosheets.

B. Experimental Setup

The experimental setup for gas sensing using the GO coated plasmonic sensor is shown in Fig. 4. The gas species (prediluted with nitrogen) flowed from cylinders into an aluminum gas chamber which contained the sensor. The sensor was illuminated from a white light source through a bifurcated fiber and the reflected light was collected by a spectrometer. Inside the chamber, the testing gas was further diluted by the carrier nitrogen gas. The gas flow rate was controlled by a mass flow controller (MFC) (GFC17, Aalborg). Ethylene with concentrations of 500 ppm, 666.66 ppm and 750 ppm, methanol with concentrations of 250 ppm, 333.33 ppm and 375 ppm and NH_3 with concentrations of 100 ppm, 117 ppm and 120 ppm were tested. A constant flow rate of dry nitrogen (10 ml/min) was maintained inside the closed chamber and flow rate of ethylene, methanol and/or NH_3 was varied to modify the concentration of the test gases at regular intervals using the MFCs. The main purpose of using dry nitrogen is to drive away moisture from the chamber, so that moisture does not produce any false spectral shifts of the sensor.

C. Gas Sensing Results

Figure 5 shows the reflection spectra of the three sensors array before and after being exposed to ethylene, methanol and

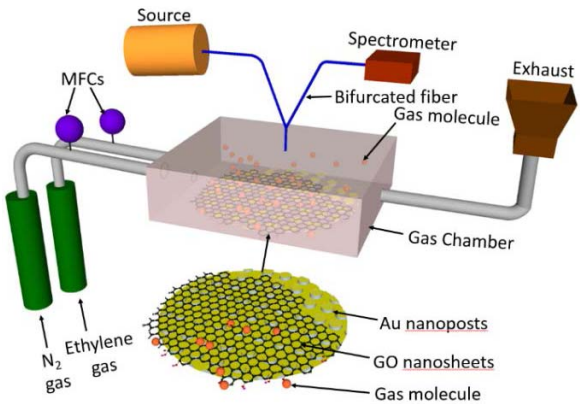

Fig. 4. Schematic illustration of experimental setup for gas sensing using GO coated plasmonic nanostructure.

NH_3 at different concentrations. As captured in (3) above, with a change in local dielectric environment and hence ε_d, a shift in resonant wavelength (λ_{SPP}) was observed. The thicker the GO coating, the higher the dielectric permittivity ε_d in the vicinity of the metal surface, and hence the higher the resonance wavelength shift. With 16.3 nm, 32.6 nm, and 48.9 nm GO coatings, resonance wavelength red-shifted from 547.1 nm to 550.1 nm, 554.2 nm and 555.25 nm respectively (Fig. 5a).

When only nitrogen was introduced into the chamber, the resonance wavelength red-shifted to 550.7 nm, 555.66 nm, and 556.1 nm for 16.3 nm, 32.6 nm, and 48.9 nm GO coatings respectively (Fig. 5a). When the sensor response was saturated in presence of nitrogen, ethylene was flown into the chamber. In the presence of ethylene gas, a red shift of the SPR wavelength occurred for all the three sensing elements. For example, with 48.9 nm GO coating, resonance wavelength shifts of 0.42 nm, 0.1 nm, and 0.17 nm were observed when the sensor was exposed to 500 ppm, 666.66 ppm, and 750 ppm of gaseous ethylene respectively. Similarly, results were obtained for methanol and NH_3 gases (Fig. 5b-c).

D. Sensitivity Studies

Sensitivity of the sensor is defined as the shift in resonance wavelength per unit change in the gas concentration. Fig. 6 shows resonance wavelength shifts with a change in gas concentration for three different thicknesses of GO coating. The sensitivities of the sensor to gaseous ethylene, methanol and NH_3 with 16.3 nm GO coating (Fig. 6) were found to be approximately 0.6 pm/ppm, 3.2 pm/ppm and 12.84 pm/ppm respectively.

A fiber-tip based FP sensor reported in literature exhibits a sensitivity of 3.53 pm/ppm to methanol vapor [40] which is close to ours. In another work, an optical fiber long-period-grating gas sensor exhibited a sensitivity of 0.2 pm/ppm for methanol gas [41] which is almost 16 fold less compared to our sensor. Also several SPR based fiber-optic ammonia gas sensors have been reported using Ag/SnO_2 thin films with a sensitivity of 2.15 nm/ppm [6], using PMMA/rGO nanocomposite with sensitivity of 1 nm/ppm [7], using Indium tin oxide (ITO) and bromocresol purple (BCP) with sensitivity of 1.891 nm/ppm [42]. The sensitivities of these sensors are higher than ours, but our plasmonic sensor offers other advantages. Firstly, it is superior in terms of fabrication methods: It employs inexpensive and simple nanomolding process to fabricate the nanopattern-based SPR structure. Moreover, in order to selectively identify gas species, by simply varying the thicknesses of the GO coatings on the sensing elements in a sensor array, it is possible to differentiate a gas from the others in a gaseous mixture, by applying pattern recognition algorithms. There is no need of changing the structures of the nanoposts that otherwise will require costly nanoscale master molds, or varying compositions of gas absorbing materials. In contrast, in the aforementioned fiber-optic SPR based sensors [6], [7], [42], different composition of coating materials needs to be employed in order to selectively detect different gas species, requiring additional fabrication steps. Finally, to our knowledge, no ethylene detection sensor has been reported based on the principle of optical resonance wavelength shift.

E. Control and Reversibility Studies

We further studied the dynamic response of the sensor coated with 32.6 nm of GO nanosheets (Fig. 7a-c). During the entire experiment, dry nitrogen was kept flowing at a constant rate into the enclosed chamber. First, when nitrogen was introduced into the chamber, the sensor response became saturated at a resonance shift of 0.2 nm (Fig. 7a). After that, the sensor was exposed to varying concentrations of ethylene gas. We observed resonance shifts of 0.15 nm and 0.23 nm for 500 ppm and 666 ppm of ethylene gas respectively (Fig. 7a). With 750 ppm and 800 ppm of gaseous ethylene, resonance shifts of 0.05 nm and 0.05 nm were observed, respectively (Fig. 7a). As the gas concentration increased to 750 ppm, less amount of resonance shift was exhibited as compared to the shift observed for 500 ppm and 666 ppm of ethylene, perhaps because the gas molecules already remaining in the GO layer inhibited further interaction and hence adsorption of newer gas molecules. Hence, at higher concentration of ethylene gas no resonance shift will be observed which implies that the sensor has a fixed operation range. With 32.6 nm GO coating, the total shifts in resonance in response to gaseous ethylene, methanol and ammonia were found to be 0.45 nm, 0.45 nm and 0.3 nm respectively (Fig. 7a-c). For comparison, we also performed the control dynamic measurements of the *bare* substrate (*without* any GO coating) (Fig. 7d-f). It is apparent from Fig. 7d that the bare sensor exhibits a much smaller total resonance shift of 0.01 nm in response to ethylene (which is 45 times smaller compared to that with GO coating). Figures 7e-f also show smaller resonance shifts in response to methanol (which is 10 times smaller compared to that with GO coating) and ammonia gases (which is 5 times smaller compared to that with GO coating). These measurements demonstrate a much higher sensitivity when coated with the GO nanosheets, thereby justifying our use of GO coating as a gas adsorption layer. The response time of the GO coated sensor, when exposed to certain concentrations (500 ppm, 666 ppm, 750 ppm, and 800 ppm) of

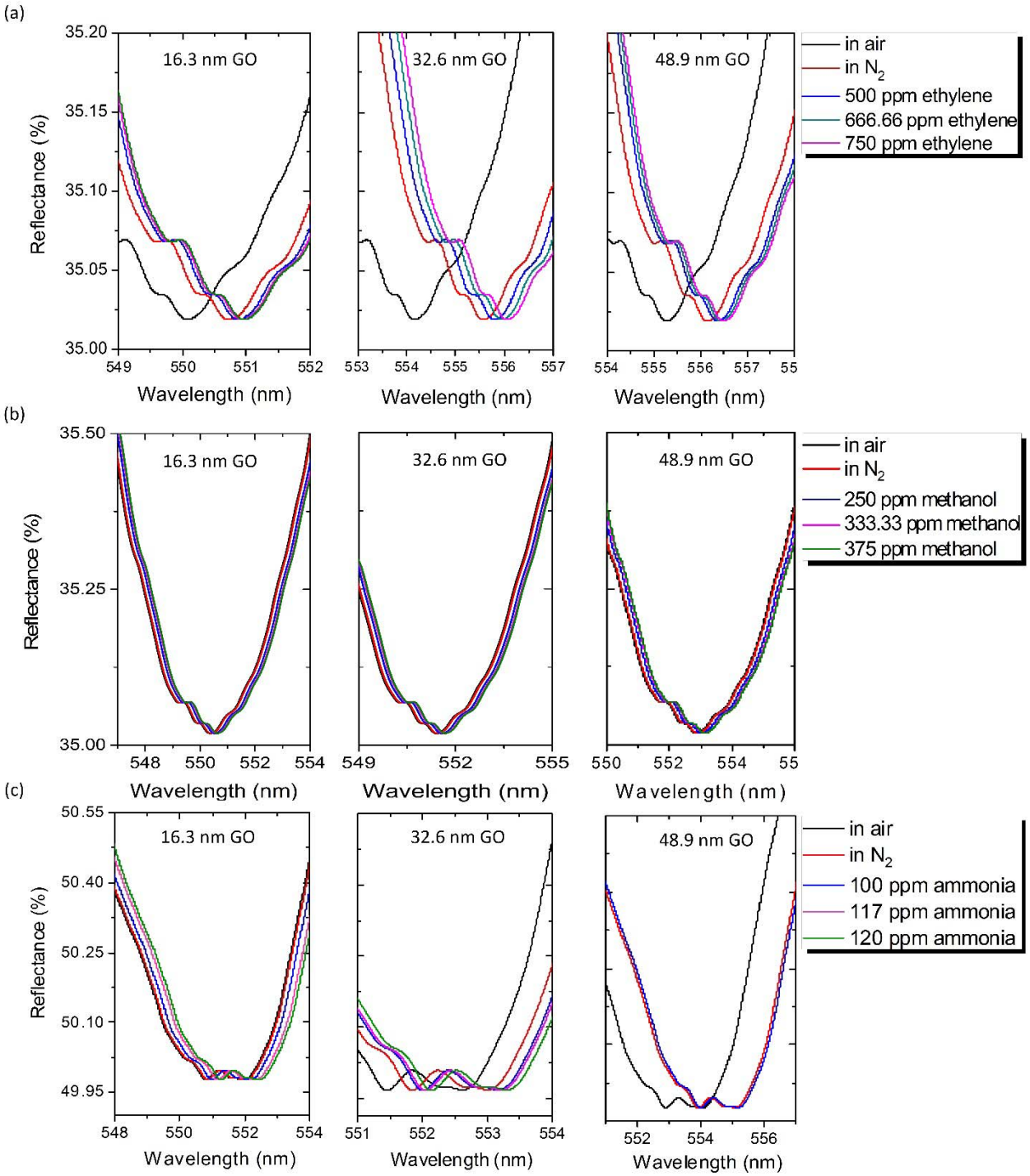

Fig. 5. Reflectance spectra of plasmonic crystal gas sensors with three different thicknesses of GO when exposed to gaseous (a) ethylene, (b) methanol and (c) NH_3.

ethylene, was approximately 40 s. The response time is mainly determined by the adsorption of gas molecules at the low or high-energy binding sites of GO nanosheets. The low energy sp^2 carbon domains lead to faster adsorption of molecules, while the vacancies, defects, and oxygen-containing functionalities act as high-energy binding sites with slower adsorption rate [26]. Also, the diffusion of the gas molecules to reach the active portion of the plasmonic nanostructure adds to the delay [43]. Weak dispersive forces allow the adsorption of gas molecules on sp^2-bonded carbon atoms of the GO layer. However, single and double hydrogen bonds are formed when gas molecules are captured at defect sites such as carboxylic acid group, requiring binding energies of several hundred meV/molecule [26]. When the gas flow (ethylene, methanol or NH_3) was turned off and the chamber was purged with dry N_2 gas, a partial recovery of the sensor was observed.

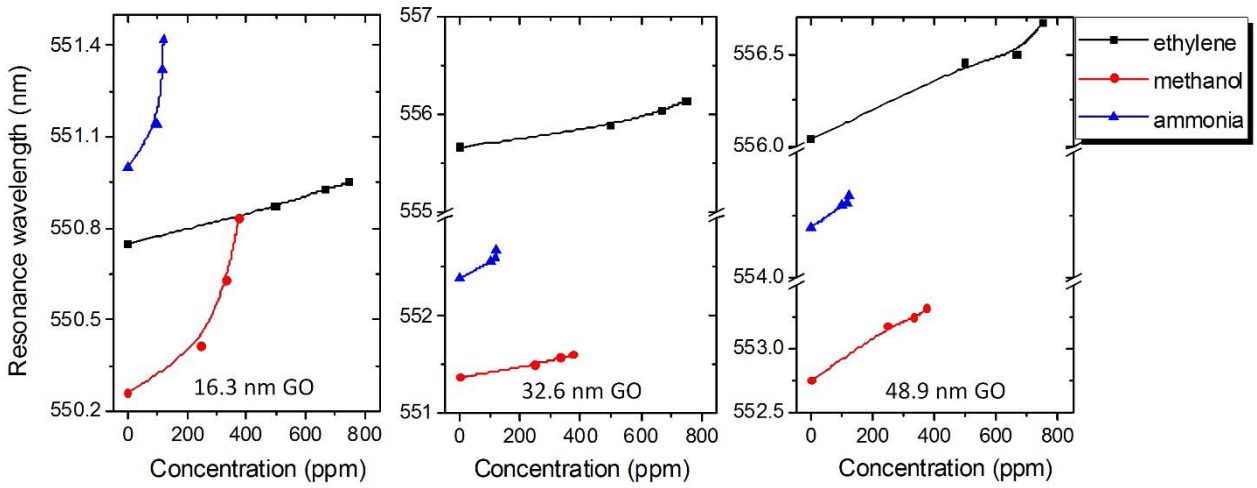

Fig. 6. Resonance wavelength shifts of three plasmonic crystal gas sensors with different thicknesses of GO as a function of concentration of gaseous ethylene, methanol and NH_3.

This is likely because only the gas molecules bound to the low-energy binding sites of GO nanosheets are released during the purging with dry N_2, while the gas molecules captured by the high-energy binding sites remain adsorbed at the GO nanosheets. This is also confirmed by noting that the resonance wavelength did not return to the baseline upon turning off the gas flow as shown in Fig. 7c. This is not unexpected, and indeed a similar behavior was observed for GO covered optical nano-antenna structure exposed to gaseous analytes in [43]. A complete release of the bounded gases from the sensor surface requires a moderate heating. In our case, to prepare for a new cycle of the dynamic response, the device was thermally treated on a hot plate at 700^0 C for 4 hours, allowing for a complete desorption of the gas molecules from the GO layer, as was confirmed experimentally by the return of the resonance wavelength to its baseline level.

F. Optimization of GO Thickness

We performed gas sensing experiments for different concentrations of GO dispersion solution in order to find an optimum GO solution providing maximum shift in resonance wavelength. It can be observed from Fig. 8 that with an increase in the concentration of GO dispersion solution, the resonance wavelength increases until a certain value of GO solution concentration, and then decreases. Experiments were conducted for gaseous ethylene in the concentration range of 500 ppm to 750 ppm and gaseous methanol in the concentration range of 250 ppm to 375 ppm. The maximum value of total shift in resonance wavelength was found to be 0.9 nm for ethylene with 0.75 mg/ml GO dispersion solution and 0.56 nm for methanol with 0.15 mg/ml GO dispersion solution.

G. Specific Gas Identification Using PCA Based Separation

The plasmonic nanostructure has been demonstrated to be sensitive to different gases such as ethylene, methanol and NH_3, but selectivity between different gases remains to be addressed owing to the interaction of GO nanosheets with all the gases which results in corresponding resonance wavelength shifts as shown in Fig. 5. This may be addressed either through modifying the sensor materials, or by applying some intelligent data analysis. Modifying the composition of gas-absorbing materials in the sensor certainly adds fabrication complexities. Hence, a multivariate analysis named PCA was used to extract selective response out of the SPR spectra of three identical sensors coated with three different thicknesses of GO. The responses of all the three sensors were collected, and a PCA method was applied to transform the data, allowing the separation of different gases, as the data corresponding a specific gas appeared in a single cluster upon the PCA based transformation. In our case, the PCA takes a multidimensional dataset and reduces it into a two-dimensional dataset, without crucial loss of information. For our experiments, the data

TABLE I
DATA MATRIX INPUT TO PCA ALGORITHM

Concentration / Gas species	Optical Resonance Wavelength (nm)		
	16.3 nm-thick GO	32.6 nm-thick GO	48.9 nm-thick GO
250 ppm / Methanol	550.41	551.50	553.17
333.33 ppm / Methanol	550.63	551.57	553.24
375 ppm / Methanol	550.83	551.60	553.31
500 ppm / Ethylene	550.87	555.80	556.40
666.66 ppm / Ethylene	550.93	556.00	556.50
750 ppm / Ethylene	550.95	556.20	556.75
100 ppm / Ammonia	551.14	552.55	554.29
117 ppm / Ammonia	551.31	552.59	554.30
120 ppm /Ammonia	551.42	552.68	554.33

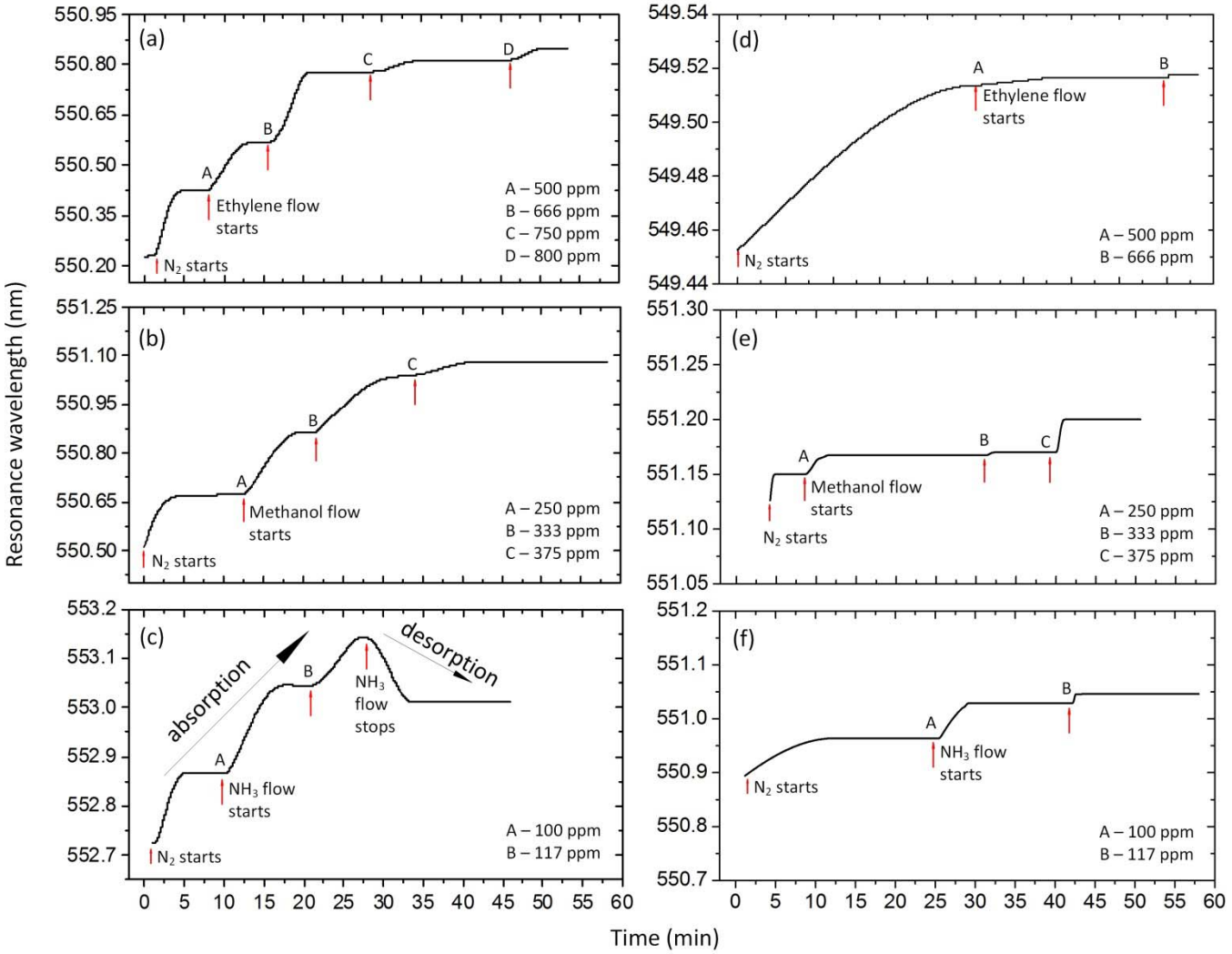

Fig. 7. Monitoring the real-time adsorption of (a) ethylene, (b) methanol and (c) ammonia into the plasmonic nanostructure with 32.6 nm thick GO coating. Control dynamic experiments in response to (d) ethylene, (e) methanol and (f) ammonia without any GO coating. A, B, C and D represent the instants at which gas was introduced into the enclosed chamber.

matrix contained the response of each sensor with a different GO thickness to a certain gas and concentration, as shown in Table I. Utilizing the PCA (see details in the PCA algorithm section of the Supplementary Materials provided at the end in an appendix), the data matrix was reduced to two principal components PC1, PC2, as plotted in Fig. 9. This figure demonstrates a clear separation of the three gas species in the three clusters, indicating the individual gases without overlap. Therefore, the PCA algorithm allows the identification of analytes with a set of three sensors with three different thicknesses of GO coated on the sensor surface. Certainly, other thickness levels can be introduced to be able to separate a larger number of species of gases. Thus, in our setting there is no need to change the compositions of the gas-absorbing films, only different GO thicknesses were needed, obtained via varying the concentrations of GO dispersion solutions using simple dip coating method.

H. Refractive Index of GO With and Without Gas

When gas molecules are adsorbed by the GO nanosheets, the refractive index of GO increases. In order to substantiate this claim, the refractive index of GO thin film was measured with and without gas, using the method developed by Minkov [44]. This method makes use of the interference effects that occur due to the reflections from the air/thin film and thin film/substrate interfaces. These dual reflections produce interference in the reflection spectrum of the film from which the refractive index of the film can be calculated [44].

We started with 2 mg of GO powder dispersed in 1 ml deionized water. The GO dispersion solution was then sprayed onto a microscope glass slide using an airbrush (Badger 350, Badger Air-Brush Co.) [45]. The substrate was next dried at room temperature for 6 hrs, which let the remaining GO sheets to form a uniform thin film on the glass slide. Next, the reflectance spectra of the GO film with and without the gaseous methanol were measured (Fig. 10). Using the method provided in [44], Table II was obtained, showing the values of the refractive indices of the GO film at different wavelengths, with and without the presence of gaseous methanol. It was observed that the refractive index of GO increases by 7.4% on average in presence of 500 ppm methanol, demonstrating the effect of gas adsorption on refractive index of GO.

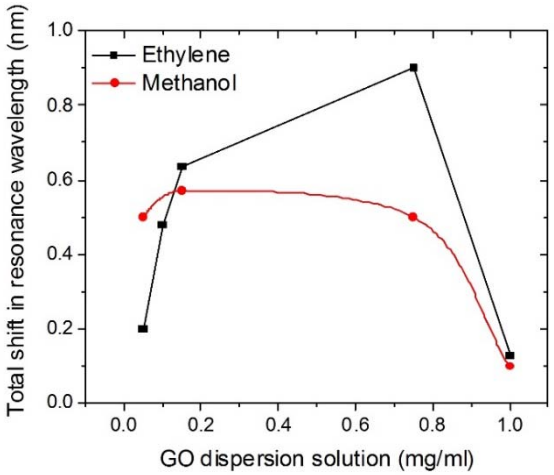

Fig. 8. Variation of total shift in resonance wavelength with the concentration of GO dispersion solution for ethylene gas concentration ranging from 500 ppm to 750 ppm and methanol gas concentration ranging from 250 ppm to 375 ppm.

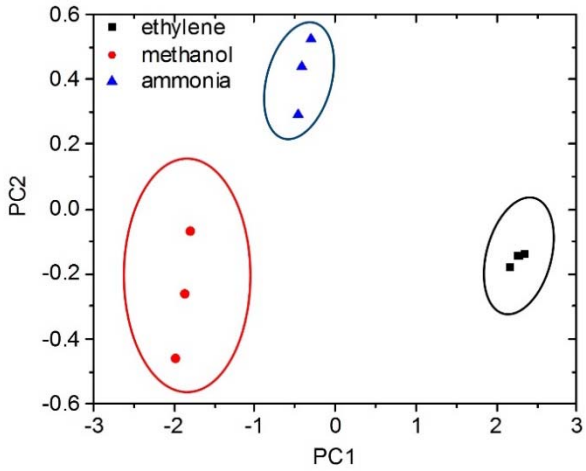

Fig. 9. Pattern analyses based on PCA using three different sensors.

Similar values of refractive index of GO in air were reported using standard spectroscopic ellipsometry [46].

V. Comparison to Related Optical Sensors

We presented a periodic nanopatterns based plasmonic gas sensor exhibiting spectral resonance shift in response to a change in surrounding refractive index in presence of gases, as well as a sensor array with varying thicknesses of GO layers to enable selective identification of gas species, aided by the PCA method. The sensor leverages the striking properties of GO nanosheets and plasmonic nanoposts to transduce gas molecule binding events into optical responses. Previously, sensors have been reported that work based on the principle of LSPR [10]. Generally, LSPR sensors display less sensitivity to changes in the bulk refractive index compared to the propagating SPR sensors [47]. The performance of the LSPR sensors also depends greatly on the nanoparticle composition, size, shape and orientation. A variety of chemical syntheses and lithographic techniques have also been adopted

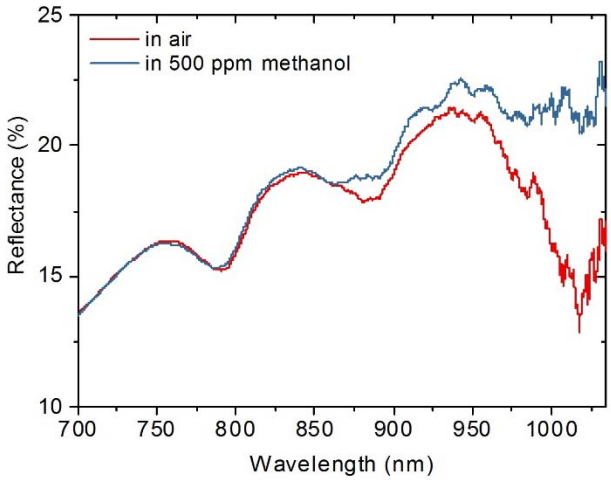

Fig. 10. Measured reflection spectra before and after the GO thin film is exposed to gaseous methanol.

TABLE II
Calculated Values of the Refractive Indices of a Thin GO Film Without and With Methanol Gas

λ (nm)	η_{GO} in air	η_{GO} in 500 ppm methanol gas
982.9	2.60	2.91
939.5	2.57	2.82
886.0	2.39	2.55
832.4	2.09	2.19
792.3	1.19	1.18

to manipulate these parameters with relatively complex and expensive fabrication methods. On the other hand, most of the existing SPR based sensors with GO layers are dedicated to biomolecules detection in liquids [19], [21]. Our sensor employs the SPR principle to probe gaseous species using a nanopost-based plasmonic structure obtained by an inexpensive nanomolding process. Our device allows for easy excitation of surface plasmons without using complex optics as in [48]. Moreover, by simply varying the thicknesses of GO layer on identical sensing elements in a sensor array, it is possible to differentiate a gas from the others in a gas mixture, using a PCA algorithm. There is no need of varying the structures of nanoposts as such that otherwise will require costly nanoscale master molds. Similarly, there is also no need of varying compositions of gas absorbing materials that are commonly used in electronic nose devices [49]–[51]. Only different concentrations of GO dispersion solutions are required to obtain different GO thicknesses via a simple dip coating. This makes the device fabrication process simpler, cost effective, yet functional.

VI. Conclusion

This paper presented a gas sensor using nanoposts-based plasmonic nanostructures coated with a thin GO layer as

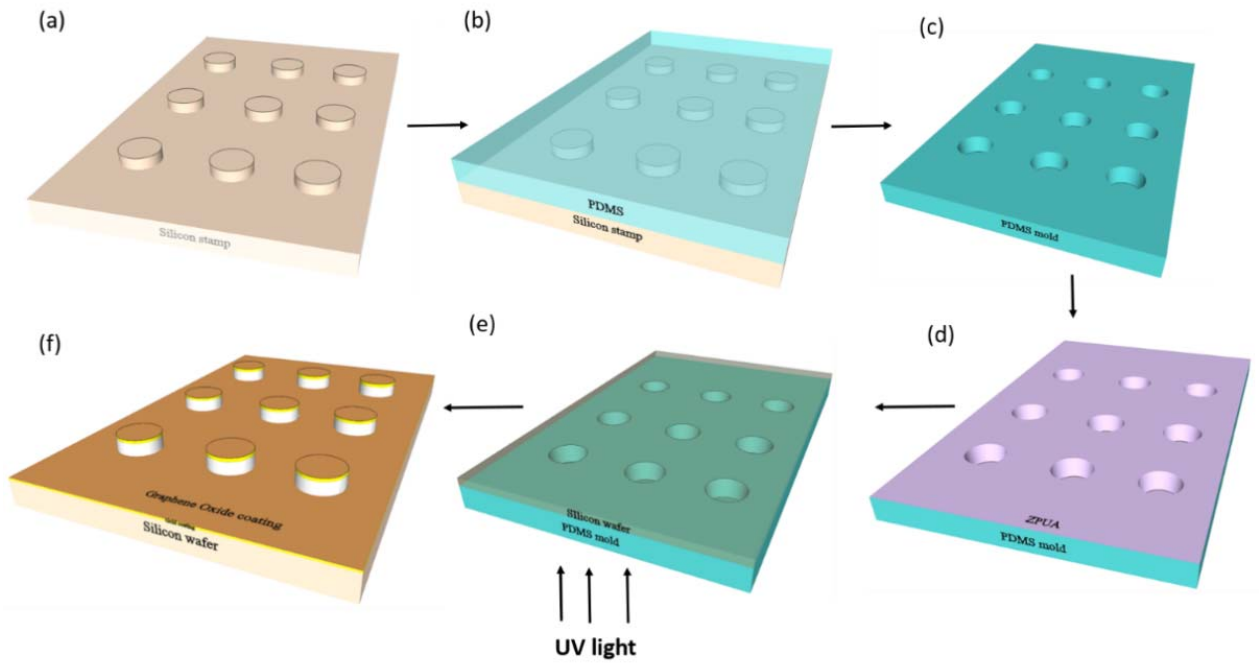

Fig. 11. Fabrication process of GO coated plasmonic crystal sensor. (a) Si master mold carrying nanoposts with period (Λ = 500 nm), diameter (d = 250 nm), and height (h = 210 nm). (b) PDMS is poured on the Si stamp. (c) PDMS is peeled off the stamp. (d) ZPUA is poured on the PDMS mold. (e) The PDMS mold is pressed against the Si wafer and exposed to UV radiation. (f) 50 nm gold coating followed by GO coating on the device.

a resonance tuning in the presence of subtle concentration changes of gas molecules. The sensor exhibits sensitivities of 0.6 pm/ppm to gaseous ethylene, 3.2 pm/ppm to methanol and 12.84 pm/ppm to NH_3 gases respectively. An array of sensors was built with the same nanoposts structure but with varying thicknesses of the GO coating. The different responses of the sensors to a gas mixture were collected and a PCA based pattern recognition algorithm was applied to generate a distinct signal cluster for each gas analyte in the mixture. The gas sensor technology reported in this paper will support detection of various gases released from a multitude of sources in the agricultural, biomedical, environmental, and manufacturing fields.

Future work will mainly focus on improving the sensor selectivity to a specific gas by coating the nanoposts based sensor array with different thicknesses of semiconducting oxides, such as ZnO_2, In_2O_3, SnO_2, etc., that show gas-specific adsorption rates. The sensing mechanism of these oxides is based on a change in electrical conductivity caused by trapping of electrons at the adsorbed gas molecules and band bending caused by these charges [52].

APPENDIX
SUPPLEMENTARY MATERIALS

A. Fabrication of Plasmonic Nanopost Array

The sensor fabrication steps [53] are shown in Fig. 11. The fabrication starts with a silicon (Si) master mold (Fig. 11a). In order to form a PDMS mold from Si master mold we followed two steps. At first the Si master mold carrying the nanopatterns was silanized with (tridecafluoro-1, 1, 2, 2- tetrahydrooctyl)-1-trichlorosilane (T2492-KG, United Chemical Technologies) in a desiccator under active vacuum for 20 min. Then, a mixture of poly (7-8% vinylmethyl-siloxane)- (dimethylsiloxane) (Gelest # VDT-731), (1, 3, 5, 7-tetravinyl-1, 3, 5, 7-tetramethylcyclotetrasiloxane) (Gelest # SIT7900.0), platinum catalyst Xylene (Gelest # SIP6831.2) and poly (25-30% methylhydro-siloxane)- (dimethylsiloxane) (Gelest # HMS-301) at the weight ratio of 3.4: 0.1: 0.05: 1 was prepared that worked as an h-PDMS precursor solution. Next, the mixture was put in a degassing chamber for 10 min to remove the air bubbles and was then spin-coated onto the Si mold at 1000 rpm for 40 s and cured at 70°C for 10 min. Subsequently, an s-PDMS precursor solution was prepared by mixing Sylgard 184 (Dow Corning) and curing agent at the weight ratio of 10: 1 and degassed in a vacuum desiccator for 20 min. After that, the s-PDMS mixture was poured onto the top surface of h-PDMS and cured on a hotplate at 65°C for 2 hrs (Fig. 11b). Finally, the PDMS slab containing a square array of nanoholes was peeled from the Si mold (Fig. 11c).

The next step was to use a UV curable polymer (ZIPCONE™UA or ZPUA) to imprint the nanoposts from the PDMS mold to a Si wafer [Fig. 11(d-e)]. At first, the Si wafer was spin coated with an adhesive layer of Transpin at 3000 rpm for 40s and subsequently heated at 200 °C for 5 min. This step is required to enhance the adhesion ability of ZPUA to Si wafer resulting in complete transfer of ZPUA nanoposts to the Si wafer. The ZPUA was dropped on the PDMS mold (Fig. 11d) and the mold was then placed on top of the Si wafer. Then the wafer was exposed to ultraviolet light for 5 min at an intensity of 3.3 mW/cm^2 (Fig. 11e). Separation

of the PDMS mold from the Si wafer resulted in nanoposts transferred to the Si wafer which was further coated with a 50 nm Au layer using e-beam evaporation.

Aqueous suspensions of GO nanosheets (2 mg/mL) were prepared by thoroughly dispersing 2 mg of the synthesized GO nanosheet flakes (purchased from Graphene Supermarket) in 1 mL of deionized water, followed by sonication at room temperature for 90 min. This solution was then diluted to make three different GO dispersion solutions (0.05 mg/ml, 0.1 mg/ml and 0.15 mg/ml). The surfaces of the three sensors were made hydrophilic by using oxygen plasma treatment before drop-coating with different amounts of GO solutions. For each coating, 100 μL/cm^2 of GO suspensions were drop coated over the sensor surface. These sensors were then dried at room temperature for one hour. The final structure is shown in Fig. 11f.

B. PCA Algorithm

The PCA algorithm was employed to find clusters in a given dataset by projecting a feature space onto a smaller subspace with minimal loss of information [54], [55]. The steps for performing PCA are listed below:

1. The entire dataset consisting of an $m \times n$ matrix is taken as input for the PCA analysis. In our case, we had a 9×3 matrix consisting of the values of resonance wavelengths for three different concentrations of ethylene, methanol and NH_3 vapors and three different thicknesses of GO as given in Table 1.
2. The mean values are computed for each row of the entire dataset. Suppose for the $m \times n$ dataset, the i^{th} row is given by, $x_{i1}, x_{i2}, x_{i3}, \ldots\ldots\ldots, x_{ij}, \ldots\ldots\ldots, x_{in}$. Then, the mean value along the i^{th} row is calculated as follows:
$$\mu_i = \frac{1}{n}\sum_{j=1}^{n} x_{ij}.$$
3. The row mean value is subtracted from all values in the row. i.e., each x_{ij} is replaced with $x_{ij} - \mu_i$. Suppose we thus get a new $m \times n$ matrix, denoted D.
4. The covariance matrix of the whole dataset is computed. The samples for the m observations (the concentrations) for the n variables (the thicknesses) are used to compute an $n \times n$ covariance matrix C, whose jk^{th} entry is given by,
$$c_{jk} = \frac{1}{m-1}\sum_{i=1}^{m}\left(D_{ij} - \bar{D}_j\right)\left(D_{ik} - \overline{D_k}\right).$$
Here D_{ij} is the ij^{th} element of matrix, and $\bar{D}_j$ is the mean value of matrix D along the j^{th} column.
5. The eigenvectors and the corresponding eigenvalues of the covariance matrix, C are computed.
6. The eigenvectors are sorted by decreasing eigenvalues. Let, W be an $n \times n$ matrix wherein the columns represent eigenvectors, sorted in the descending order of eigenvalues.
7. The matrix W is used to transform the samples using,
$$y = WD^T,$$
where y is the transformed $n \times m$ dimensional sample in the new space.
8. Finally, the first k rows of the matrix y are chosen that correspond to first k eigenvectors with the largest eigenvalues. (For our case $k = 3$ since three gases in the mixture.)

Following the steps 1-8 described above, the matrix in Table 1 was reduced to the two principal components PC1, PC2 as plotted in Fig. 9. The plot clearly shows three different separated clusters for the three gas species.

ACKNOWLEDGMENT

The authors would like to thank Qiugu Wang for assistance with initial simulation and inputs on theoretical understanding, Seval Oren for running the SEM, Wentai Wang for assisting with the fabrication process, Prof. Meng Lu and Prof. Robert J. Weber for sensor related discussions. All the above names are affiliated with the Iowa State University, Department of Electrical and Computer Engineering.

REFERENCES

[1] B. Esser, J. M. Schnorr, and T. M. Swager, "Selective detection of ethylene gas using carbon nanotube-based devices: Utility in determination of fruit ripeness," *Angew. Chem. Int. Ed.*, vol. 51, no. 23, pp. 5752–5756, 2012.

[2] G. E. Schaller, "Ethylene and the regulation of plant development," *BMC Biol.*, vol. 10, no. 1, p. 9, 2012.

[3] R. Fall and A. A. Benson, "Leaf methanol—The simplest natural product from plants," *Trends Plant Sci.*, vol. 1, no. 9, pp. 296–301, 1996.

[4] W. Jud *et al.*, "Effects of heat and drought stress on post-illumination bursts of volatile organic compounds in isoprene-emitting and non-emitting poplar," *Plant, Cell Environ.*, vol. 39, no. 9, pp. 1204–1215, 2016.

[5] N. G. Patel, P. D. Patel, and V. S. Vaishnav, "Indium tin oxide (ITO) thin film gas sensor for detection of methanol at room temperature," *Sens. Actuators B, Chem.*, vol. 96, no. 1, pp. 180–189, 2003.

[6] A. Pathak, S. K. Mishra, and B. D. Gupta, "Fiber-optic ammonia sensor using Ag/SnO_2 thin films: Optimization of thickness of SnO_2 film using electric field distribution and reaction factor," *Appl. Opt.*, vol. 54, no. 29, pp. 8712–8721, 2015.

[7] S. K. Mishra, S. N. Tripathi, V. Choudhary, and B. D. Gupta, "SPR based fibre optic ammonia gas sensor utilizing nanocomposite film of PMMA/reduced graphene oxide prepared by *in situ* polymerization," *Sens. Actuators B, Chem.*, vol. 199, pp. 190–200, Aug. 2014.

[8] S. K. Mishra, D. Kumari, and B. D. Gupta, "Surface plasmon resonance based fiber optic ammonia gas sensor using ITO and polyaniline," *Sens. Actuators B, Chem.*, vols. 171–172, pp. 976–983, Aug./Sep. 2012.

[9] T. E. Brook and R. Narayanaswamy, "Polymeric films in optical gas sensors," *Sens. Actuators B, Chem.*, vol. 51, no. 1, pp. 77–83, 1998.

[10] C. S. Cheng, Y. Q. Chen, and C. J. Lu, "Organic vapour sensing using localized surface plasmon resonance spectrum of metallic nanoparticles self assemble monolayer," *Talanta*, vol. 73, pp. 358–365, Apr. 2007.

[11] M. Cittadini, M. Bersani, F. Perrozzi, L. Ottaviano, W. Wlodarski, and A. Martucci, "Graphene oxide coupled with gold nanoparticles for localized surface plasmon resonance based gas sensor," *Carbon*, vol. 69, pp. 452–459, Apr. 2014.

[12] S. K. Mishra and B. D. Gupta, "Surface plasmon resonance-based fiber optic chlorine gas sensor utilizing indium-oxide-doped tin oxide film," *J. Lightw. Technol.*, vol. 33, no. 13, pp. 2770–2776, Jul. 1, 2015.

[13] S. K. Mishra, S. N. Tripathi, V. Choudhary, and B. D. Gupta, "Surface plasmon resonance-based fiber optic methane gas sensor utilizing graphene-carbon nanotubes-poly(methyl methacrylate) hybrid nanocomposite," *Plasmonics*, vol. 10, no. 5, pp. 1147–1157, 2015.

[14] S. K. Mishra, S. P. Usha, and B. D. Gupta, "A lossy mode resonance-based fiber optic hydrogen gas sensor for room temperature using coatings of ITO thin film and nanoparticles," *Meas. Sci. Technol.*, vol. 27, no. 4, p. 045103, 2016.

[15] H. Xu, P. Wu, C. Zhu, A. Elbaz, and Z. Z. Gu, "Photonic crystal for gas sensing," *J. Mater. Chem. C*, vol. 1, no. 38, pp. 6087–6098, 2013.
[16] N. A. Yebo, P. Lommens, Z. Hens, and R. Baets, "An integrated optic ethanol vapor sensor based on a silicon-on-insulator microring resonator coated with a porous ZnO film," *Opt. Exp.*, vol. 18, no. 11, pp. 11859–11866, 2010.
[17] Z. Han *et al.*, "On-chip mid-infrared gas detection using chalcogenide glass waveguide," *Appl. Phys. Lett.*, vol. 108, no. 14, p. 141106, 2016.
[18] J. N. Anker, W. P. Hall, O. Lyandres, N. C. Shah, J. Zhao, and R. P. Van Duyne, "Biosensing with plasmonic nanosensors," *Nature Mater.*, vol. 7, no. 6, pp. 442–453, Jun. 2008.
[19] N.-F. Chiu, T.-Y. Huang, and H.-C. Lai, *Graphene Oxide Based Surface Plasmon Resonance Biosensors*. Rijeka, Croatia: InTech, 2013, ch. 8.
[20] J. I. L. Chen, Y. Chen, and D. S. Ginger, "Plasmonic nanoparticle dimers for optical sensing of DNA in complex media," *J. Amer. Chem. Soc.*, vol. 132, no. 28, pp. 9600–9601, 2010.
[21] M. A. Ali, S. Tabassum, Q. Wang, Y. Wang, R. Kumar, and L. Dong, "Plasmonic-electrochemical dual modality microfluidic sensor for cancer biomarker detection," in *Proc. IEEE 30th Int. Conf. Micro Electro Mech. Syst. (MEMS)*, Las Vegas, NV, USA, Jan. 2017, pp. 390–393.
[22] K. Aslan, J. R. Lakowicz, and C. D. Geddes, "Nanogold plasmon resonance-based glucose sensing. 2. Wavelength-ratiometric resonance light scattering," *Anal. Chem.*, vol. 77, no. 7, pp. 2007–2014, 2005.
[23] D. Chen, H. Feng, and J. Li, "Graphene oxide: Preparation, functionalization, and electrochemical applications," *Chem. Rev.*, vol. 112, no. 11, pp. 6027–6053, 2012.
[24] S. S. Nanda, D. K. Yi, and K. Kim, "Study of antibacterial mechanism of graphene oxide using Raman spectroscopy," *Sci. Rep.*, vol. 6, p. 28443, Jun. 2016.
[25] G. Lu, L. E. Ocola, and J. Chen, "Gas detection using low-temperature reduced graphene oxide sheets," *Appl. Phys. Lett.*, vol. 94, no. 8, pp. 083111-1–083111-3, Feb. 2009.
[26] J. T. Robinson, F. K. Perkins, E. S. Snow, Z. Wei, and P. E. Sheehan, "Reduced graphene oxide molecular sensors," *Nano Lett.*, vol. 8, no. 10, pp. 3137–3140, 2008.
[27] S. Tabassum *et al.*, "Plasmonic crystal gas sensor incorporating graphene oxide for detection of volatile organic compounds," in *Proc. IEEE 29th Int. Conf. Micro Electro Mech. Syst. (MEMS)*, Shanghai, China, Jan. 2016, pp. 913–916.
[28] N. A. Joy *et al.*, "Selective plasmonic gas sensing: H_2, NO_2, and CO spectral discrimination by a single Au-CeO_2 nanocomposite film," *Anal. Chem.*, vol. 84, no. 11, pp. 5025–5034, 2012.
[29] C. Y. Lee and M. S. Strano, "Understanding the dynamics of signal transduction for adsorption of gases and vapors on carbon nanotube sensors," *Langmuir*, vol. 21, no. 11, pp. 5192–5196, 2005.
[30] A. Vakil and N. Engheta, "Transformation optics using graphene," *Science*, vol. 332, no. 6035, pp. 1291–1294, 2011.
[31] B. Yao *et al.*, "All-optical Mach–Zehnder interferometric NH_3 gas sensor based on graphene/microfiber hybrid waveguide," *Sens. Actuators B, Chem.*, vol. 194, pp. 142–148, Apr. 2014.
[32] H. F. Ghaemi, T. Thio, D. E. Grupp, T. W. Ebbesen, and H. J. Lezec, "Surface plasmons enhance optical transmission through subwavelength holes," *Phys. Rev. B, Condens. Matter*, vol. 58, no. 11, pp. 6779–6782, 1998.
[33] E. D. Palik, *Handbook of Optical Constants of Solids*. New York, NY, USA: Academic, 1985.
[34] Y. Shen *et al.*, "Plasmonic gold mushroom arrays with refractive index sensing figures of merit approaching the theoretical limit," *Nature Commun.*, vol. 4, p. 2381, Aug. 2013.
[35] J. Xu *et al.*, "Understanding the effects of dielectric medium, substrate, and depth on electric fields and SERS of quasi-3D plasmonic nanostructures," *Opt. Exp.*, vol. 19, no. 21, pp. 20493–20505, 2011.
[36] Q. Wang, W. Han, P. Liu, and L. Dong, "Electrically tunable quasi-3-D mushroom plasmonic crystal," *J. Lightw. Technol.*, vol. 34, no. 9, pp. 2175–2181, May 1, 2016.
[37] M. Seredych and T. J. Bandosz, "Mechanism of ammonia retention on graphite oxides: Role of surface chemistry and structure," *J. Phys. Chem. C*, vol. 111, no. 43, pp. 15596–15604, 2007.
[38] D. R. Dreyer, S. Park, C. W. Bielawski, and R. S. Ruoff, "The chemistry of graphene oxide," *Chem. Soc. Rev.*, vol. 39, no. 1, pp. 228–240, 2010.
[39] A. J. Roche, "Ch08 Reacns of alkenes (landscape).doc," Rutgers Univ., New Brunswick, NJ, USA, Tech. Rep.
[40] J. Liu, Y. Sun, and X. Fan, "Highly versatile fiber-based optical Fabry-Pérot gas sensor," *Opt. Exp.*, vol. 17, no. 4, pp. 2731–2738, 2009.
[41] J. Hromadka, B. Tokay, S. James, R. P. Tatam, and S. Korposh, "Optical fibre long period grating gas sensor modified with metal organic framework thin films," *Sens. Actuators B, Chem.*, vol. 221, pp. 891–899, Dec. 2015.
[42] S. K. Mishra, S. Bhardwaj, and B. D. Gupta, "Surface plasmon resonance-based fiber optic sensor for the detection of low concentrations of ammonia gas," *IEEE Sensors J.*, vol. 15, no. 2, pp. 1235–1239, Feb. 2015.
[43] B. Mehta, K. D. Benkstein, S. Semancik, and M. E. Zaghloul, "Gas sensing with bare and graphene-covered optical nano-antenna structures," *Sci. Rep.*, vol. 6, p. 21287, Feb. 2016.
[44] D. A. Minkov, "Calculation of the optical constants of a thin layer upon a transparent substrate from the reflection spectrum," *J. Phys. D, Appl. Phys.*, vol. 22, no. 8, pp. 1157–1161, 1989.
[45] S. H. Fei, W. Can, S. Z. Pei, Z. Y. Liang, J. K. Juan, and Y. G. Zhen, "Transparent conductive reduced grahene oxide thin films produced by spray coating," *Sci. China-Phys. Mech. Astron.*, vol. 58, no. 1, p. 014202, 2015.
[46] V. G. Kravets *et al.*, "Engineering optical properties of a graphene oxide metamaterial assembled in microfluidic channels," *Opt. Exp.*, vol. 23, no. 2, pp. 1265–1275, 2015.
[47] A. J. Haes and R. P. van Duyne, "A unified view of propagating and localized surface plasmon resonance biosensors," *Anal. Bioanal. Chem.*, vol. 379, nos. 7–8, pp. 920–930, 2004.
[48] E. Kretschmann and H. Raether, "Radiative decay of non radiative surface plasmons excited by light," *Zeitschrift Naturforschung A*, vol. 23, no. 12, pp. 2135–2136, 1968.
[49] A. Berna, "Metal oxide sensors for electronic noses and their application to food analysis," *Sensors*, vol. 10, no. 4, pp. 3882–3910, 2010.
[50] N. E. Barbri, A. Amari, M. Vinaixa, B. Bouchikhi, X. Correig, and E. Llobet, "Building of a metal oxide gas sensor-based electronic nose to assess the freshness of sardines under cold storage," *Sens. Actuators B, Chem.*, vol. 128, no. 1, pp. 235–244, 2007.
[51] M. O'Connell, G. Valdora, G. Peltzer, and R. M. Negri, "A practical approach for fish freshness determinations using a portable electronic nose," *Sens. Actuators B, Chem.*, vol. 80, no. 2, pp. 149–154, 2001.
[52] C. Wang, L. Yin, L. Zhang, D. Xiang, and R. Gao, "Metal oxide gas sensors: Sensitivity and influencing factors," *Sensors*, vol. 10, no. 3, pp. 2088–2106, Jan. 2010.
[53] S. Tabassum *et al.*, "Patterning of nanophotonic structures at optical fiber tip for refractive index sensing," in *Proc. IEEE SENSORS*, Orlando, FL, USA, Oct. 2016, pp. 1–3.
[54] J. E. Jackson, *A User's Guide to Principal Components*. Hoboken, NJ, USA: Wiley, 2003.
[55] I. T. Jolliffe, *Principal Component Analysis*. New York, NY, USA: Springer, 2002.

Shawana Tabassum received the B.S. degree in electrical engineering from the Bangladesh University of Engineering and Technology, Bangladesh, in 2014. She is currently pursuing the Ph.D. degree in electrical engineering with Iowa State University. Her research interests include optical MEMS sensors for sustainable agriculture.

Ratnesh Kumar (F'07) received the B.Tech. degree in electrical engineering from IIT Kanpur, India, in 1987, and the M.S. and Ph.D. degrees in electrical and computer engineering from The University of Texas at Austin, Austin, TX, USA, in 1989 and 1991, respectively. He has been a Professor of Electrical and Computer Engineering at Iowa State University since 2002. Prior to this, he was on the faculty of the University of Kentucky from 1991 to 2002 in electrical and computer engineering, and has held visiting positions with the University of Maryland, the Applied Research Laboratory (at Penn State University), NASA Ames, the Idaho National Laboratory, the United Technologies Research Center, and the Air Force Research Laboratory. He received the Gold Medals for the Best EE Undergrad and the Best All Rounder from IIT Kanpur, and the Best Dissertation Award from UT Austin. He is a Distinguished Lecturer for the IEEE Control Systems Society, Best Paper Award recipient from the IEEE TRANSACTIONS ON AUTOMATION SCIENCE AND ENGINEERING.

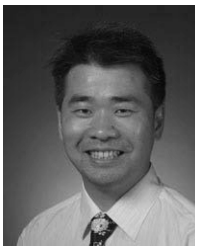

Liang Dong received the Ph.D. degree in electronic science and technology from the Institute of Microelectronics, Tsinghua University, Beijing, China, in 2004. He is currently an Associate Professor with the Department of Electrical and Computer Engineering, a Courtesy Associate Professor with the Department of Chemical and Biological Engineering, and an Associate Director of Microelectronics Research Center at Iowa State University (ISU). He is also an Associate of DOE's Ames Laboratory, and a Faculty Scholar of the Plant Sciences Institute with ISU. From 2004 to 2007, he was a Post-Doctoral Research Associate with the Department of Electrical and Computer Engineering, University of Wisconsin-Madison, Madison, WI, USA. His current research interests include MEMS/NEMS, microfluidic devices, sensors, micro/nano-optics, and micro/nanomanufacturing, and their applications in sustainable agriculture and environments, plant sciences, biomedicine, and Internet of Things. He was a recipient of the National Science Foundation CAREER Award, the Early Career Engineering Faculty Research Award, the Harpole-Pentair Developing Faculty Award, and the Warren B. Boast Undergraduate Teaching Award at ISU, and the Academic Rising Star Award from Tsinghua University, and the Top 100 National Outstanding Doctoral Dissertation Award in China. He is an Editorial Board Member for the journal scientific reports, and a Guest Editor of the journals, such as *Micromachines* and the *IEEE Nanotechnology Magazine*.